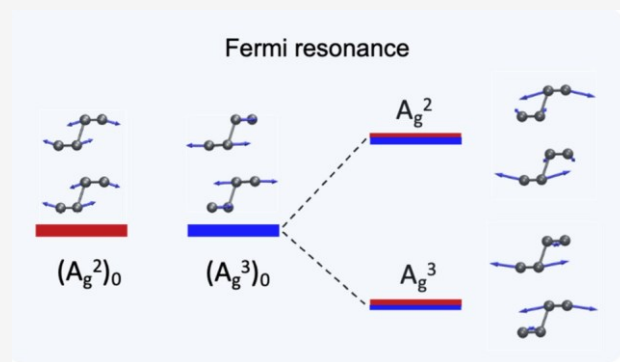# Vibrational Fermi Resonance in Atomically Thin Black Phosphorus

Nannan Mao, Shenyang Huang, Luiz Gustavo Pimenta Martins, Hugen Yan, Xi Ling, Liangbo Liang,* Jing Kong,* and William A. Tisdale*

ABSTRACT: Fermi resonance is a phenomenon involving the hybridization of two coincidentally quasi-degenerate states that is observed in the vibrational or electronic spectra of molecules. Despite numerous examples in molecular systems, vibrational Fermi resonances in dispersive semiconducting systems remain largely unexplored due to the rarity of occurrence. Here we report a vibrational Fermi resonance in atomically thin black phosphorus. The Fermi resonance arises via anharmonic mixing of a fundamental Raman mode and a Davydov component of an infrared mode, leading to a doublet with mixed character. The extent of Fermi coupling can be modulated by the application of external biaxial strain. The consequences of Fermi hybridization are revealed by electronic resonance effects in the thickness-dependent and

excitation-wavelength-dependent Raman spectrum, which is predicted by *ab initio* hybrid functional simulations including excitonic interactions. This work reveals new insight into electron−phonon coupling in black phosphorus and demonstrates a novel method for modulating Fermi resonances in 2D semiconductors.

KEYWORDS: *vibrational Fermi resonance, electrotonic resonance, Raman spectroscopy, few-layer black phosphorus*

Resonant coupling among molecular vibrations, electronic levels, and other quasiparticles plays an important role in the fundamental understanding of molecular and electronic spectra.[1,2] Resonant coupling is also responsible for a variety of phenomena in solid state systems, including polaritons,[3] hybrid magnon-phonons,[4,5] and scars in optical cavities.[6,7] A notable example in molecular systems known as a "Fermi resonance" arises from the anharmonic coupling between two vibrational modes that coincidentally have similar frequency.[8−11] For the Fermi resonance to be observed, the modes must be nearly degenerate in energy, possess similar symmetry properties, and be localized within the same molecular framework region.[9,10] Resonant coupling between these modes leads to an avoided crossing in frequency space (also called level repulsion) and the observation of changing relative peak intensities in electronic or vibrational spectra due to redistribution of oscillator strength between the two modes.[2,12,13] Since the vibrational modes in molecular systems are highly sensitive to variations in the local environment, it has been demonstrated that the strength of Fermi coupling can be modulated by a variation of intermolecular forces,[14−16] isotopic substitution,[17] and changing temperature[18,19] or pressure.[20,21] As a result, Fermi resonances hold significant importance not only in probing fundamental chemical processes�including hydrogen bonding,[15] solvent effects,[11] isotopic substitution,[17] ion−molecule interactions,[22] and intramolecular energy trans-

fer[23]�but also for practical applications in sensing,[17] dielectric optical cavities,[7] and spintronics.[4]

Though there are many reported examples of the Fermi resonance effect, most of these studies have been limited to molecular systems,[1,2,14−16] while Fermi resonance effects in dispersive semiconducting systems remain largely unexplored. In atomically thin semiconductors�where excitonic effects can exert a profound influence on electron−phonon coupling[24−28]�the effects of Fermi coupling on the vibrational and infrared spectrum are expected to be particularly pronounced.

Black phosphorus (BP), a two-dimensional elemental semiconductor exhibiting quantized electronic structure and tightly bound excitons, is a promising candidate for optoelectronics and an intriguing semiconducting system for exciton-related photophysics.[29−32] In this study, we report the observation of a vibrational Fermi resonance in atomically thin black phosphorus. The resulting Fermi doublet arises from Fermi coupling between a fundamental Raman mode (A_g^2)
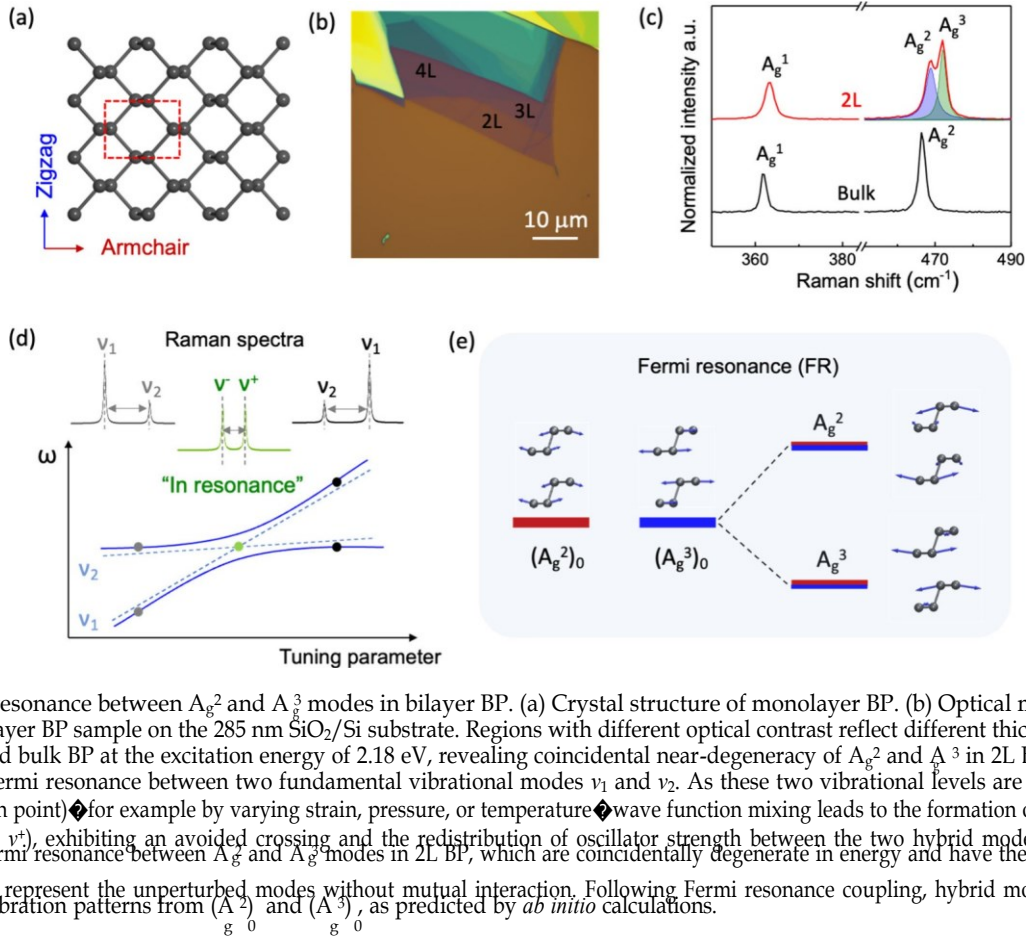
Figure 1. Fermi resonance between A_g^2 and A_g^3 modes in bilayer BP. (a) Crystal structure of monolayer BP. (b) Optical micrograph of an exfoliated few-layer BP sample on the 285 nm SiO_2/Si substrate. Regions with different optical contrast reflect different thickness. (c) Raman spectra of 2L and bulk BP at the excitation energy of 2.18 eV, revealing coincidental near-degeneracy of A_g^2 and A_g^3 in 2L BP. (d) Schematic illustration of Fermi resonance between two fundamental vibrational modes v_1 and v_2. As these two vibrational levels are tuned to be near degenerate (green point)�for example by varying strain, pressure, or temperature�wave function mixing leads to the formation of new vibrational doublets (v^- and v^+), exhibiting an avoided crossing and the redistribution of oscillator strength between the two hybrid modes. (e) Schematic illustration of Fermi resonance between A_g^2 and A_g^3 modes in 2L BP, which are coincidentally degenerate in energy and have the same symmetry. $(A_g^2)_0$ and $(A_g^3)_0$ represent the unperturbed modes without mutual interaction. Following Fermi resonance coupling, hybrid modes A_g^2 and A_g^3 show distinct vibration patterns from $(A_g^2)_0$ and $(A_g^3)_0$, as predicted by *ab initio* calculations.

and a Davydov component (A_g^3) of an infrared mode (B_{2u}). The strong coupling between these modes is a result of quantum mechanical mixing of their wave functions, which is validated by the marked change of Raman intensity due to their hybridization. Furthermore, we show that biaxial strain can be used to modulate the frequency and coupling strength of these modes, which provides direct evidence of accidental degeneracy as the origin of the Fermi resonance. Notably, the Fermi doublets exhibit unusual thickness-dependent electronic resonance effects, which are explained by hybrid functional simulations that consider exciton−phonon coupling.

FERMI RESONANCE BETWEEN A_G^2 AND A_G^3 MODES IN ATOMICALLY THIN BP

With four phosphorus atoms in the primitive cell (Figure 1a), bulk black phosphorus (point group D_{2h}^{18}) has nine optical branches in its phonon dispersion.[33,34] Notably, the A_g^2 mode (Raman active) and B_{2u} mode (IR-active) show nearly identical frequencies, a coincidental situation referred to as "accidental degeneracy",[35] as revealed by Raman and IR spectroscopic measurements.[36−38] For this study, few-layer BP samples were prepared by mechanical exfoliation onto a 285 nm SiO_2/Si substrate in an argon glovebox (Figure 1b). Raman spectra were collected with incident (e_i) and collection polarizations (e_s) aligned parallel to the armchair (AC) crystalline orientation (e_i //e_s //AC). BP samples were sealed in an argon-filled container during the Raman measurement to avoid possible oxidation.

Figure 1c displays the typical Raman spectra of bulk and 2L BP with e_i //e_s //AC configuration. In bulk BP, two characteristic Raman peaks were observed: A_g^1 (362.0 cm^{-1}) and A_g^2 (467.7 cm^{-1}). However, in 2L BP, a new strong Raman peak emerges at the high-frequency shoulder of A_g^2. This peak is close in frequency to the A_g^2 mode and has been previously identified as the Raman-active component of a Davydov-split infrared-active (B_{2u}) mode.[39] It has similar symmetry as the A_g^2 mode and is marked as A_g^3 in Figure 1c.

In few-layer van der Waals materials, coupling between vibrational modes in adjacent layers leads to renormalization of the vibrational spectra, known as Davydov splitting.[39,40] Some of the Davydov components of an infrared-active mode in few-layer layered materials become Raman active due to broken translational symmetry at the two-dimensional limit.[41] However, these Davydov modes typically exhibit considerably weaker Raman intensity[42] than normal Raman-active modes. For the case of 2L BP, the bulk infrared-active B_{2u} mode undergoes Davydov splitting into a Raman-active A_g^3 mode and an IR-active B_{2u} mode.[39] Surprisingly, the A_g^3 mode in 2L BP consistently shows a stronger Raman intensity than that expected for a Davydov-splittingcomponent of an infrared-active mode, appearing comparable to the normal Raman-active A_g^2 mode across a wide range of excitation wavelengths. This observation suggests that another mechanism, a Fermi resonance, is responsible for the enhanced Raman intensity of the A_g^3 mode in 2L BP.

Fermi resonance is an anharmonic coupling that occurs between two vibrational modes (denoted as v_1 and v_2, Figure 1d) that are nearly degenerate in energy and have the same symmetry. Classically, Fermi resonances have been commonly observed between fundamental modes and overtone modes in
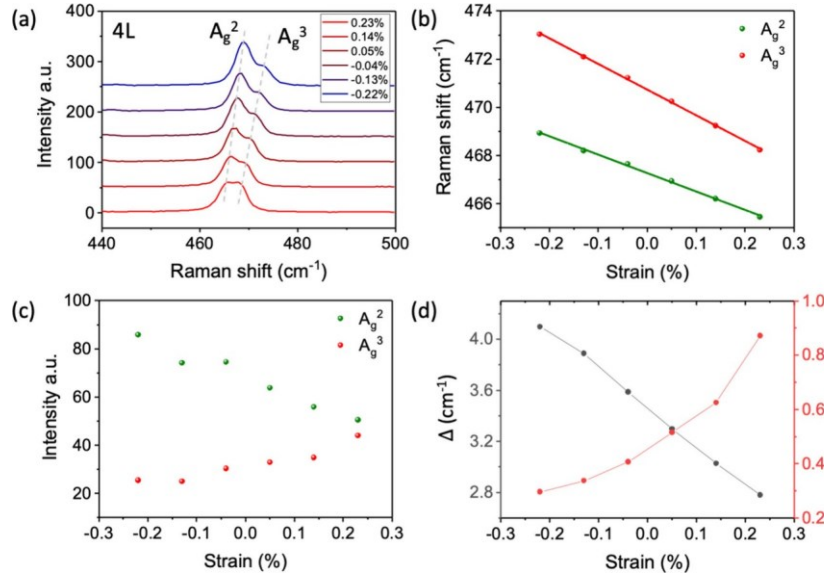
Figure 2. Strain-modulated Fermi resonance in 4L BP. (a) Biaxial strain-dependent Raman spectra of 4L BP on the polypropylene substrate, revealing tunable degeneracy between A_g^2 and A_g^3 modes. The evolutions of (b) frequencies and (c) intensities of A_g^2 and A_g^3 modes as a function of the biaxial tensile (>0) and compressive strain (<0). (d) The evolutions of their frequency difference and intensity ratio (A_g^3/A_g^2) as a function of the biaxial strain.

molecular systems such as CO_2.[8,9] Strong coupling between these two modes is facilitated by the mixing of their wave functions, leading to a lifting of their frequency degeneracy (yielding v^- and v^+) and a redistribution of oscillator strength between them.[2,12,13] The generated doublets are described as a linear combination of the unperturbed modes.[12] Under strong coupling conditions, the two modes involved in Fermi coupling usually appear with comparable intensity in vibrational spectra and exhibit a frequency splitting.[21] The A_g^2 and A_g^3 modes in 2L BP fulfill the conditions of Fermi resonance, giving rise to distinct vibration patterns compared to their parent modes, $(A_g^2)_0$ and $(A_g^3)_0$, as illustrated in Figure 1e.

First-principles density functional theory (DFT) tends to underestimate the frequency of the A_g^2 mode, and does not adequately capture the accidental degeneracy of A_g^2 and A_g^3 or strong coupling between them.[35] Consequently, the vibrational patterns calculated in this way represent the unperturbed modes. However, when employing DFT with a more accurate hybrid functional method, as reported by Sun et al.,[35] we not only accurately predict the frequency of the A_g^2 mode but also capture the Fermi resonance coupling between A_g^2 and A_g^3 modes, as indicated in Figure 1e (see more details in the DFT Simulation section in the Supporting Information).

Direct Evidence of Fermi Resonance: Strain-Modulated Raman Spectra. The coupling strength between the two vibrational modes contributing to a Fermi resonance can be modulated by external parameters, such as strain,[35] pressure,[20,21] and temperature.[18,19,21] As the unperturbed frequencies of two such states shift in response to external parameters and become closer to each other, the anharmonic coupling between them becomes more pronounced (as depicted in Figure 1d). To demonstrate the Fermi coupling between A_g^2 and A_g^3 modes, we applied biaxial strain to modulate their Raman frequencies and mutual interaction in 2L−8L BP.[43] Biaxial strain here was introduced via thermal expansion or compression of the polypropylene substrate. Taking 4L BP as an example (Figure 2a−c), as the biaxial strain evolves from compressive to tensile (−0.22% < ε <

0.23%) strain, a clear red shift trend is observed on both modes. However, the A_g^3 mode undergoes a faster shift compared to the A_g^2 mode. Moreover, the intensity of A_g^2 decreases while that of A_g^3 increases. As the frequency of A_g^3 becomes closer to that of the A_g^2 mode, their intensity ratio (A_g^3/A_g^2) approaches 1 (Figure 2b−d), which is consistent with the expected behavior of Fermi resonance. This observation provides direct evidence of Fermi coupling between the A_g^2 and A_g^3 modes.

Similar strain modulation was also observed on 2L and 6L BP (Figures S1−S2, Supporting Information). According to perturbation theory,[11] the Fermi coupling coefficient W between the Fermi doublets is estimated by $W = \frac{\sqrt{R}\Delta}{R+1}$, where R is the Raman intensity ratio between the Fermi doublets (A_g^3/A_g^2) and Δ denotes their energy separation.[11] Stronger Fermi coupling gives rise to larger energy separation Δ at maximum resonance, with respect to the energy separation of the unperturbed vibrational modes. At maximum resonance, $R \approx 1$ and Δ reaches its minimum observed value (δ), at which point $W = \frac{\delta}{2}$. We find that the maximum coupling coefficient W between A_g^2 and A_g^3 decreases as the thickness of BP increases from $W = 1.5$ cm^{-1} for 2L BP to $W = 1.2$ cm^{-1} for 6L BP (Table S1, Figure S1).

Electronic Resonance Effect on Fermi Doublets. Electronic and excitonic resonance effects can exert a significant influence on phonon vibrations through electron−phonon coupling.[24−28] BP exhibits a quantized band structure featuring thickness-dependent direct bandgap and above-bandgap transitions in the near-IR and visible region.[29−32] Consequently, the combination of Fermi resonance and strong electronic resonance effects is expected to have a dramatic effect on the observed Raman spectrum in few-layer BP.

To explore the interplay of electronic/excitonic and Fermi resonances, we performed Raman measurement on 2L−4L BP using 15 different excitation laser lines spanning from 1.92 to 2.73 eV. The chosen laser lines effectively cover most of the subband transitions in few-layer BP.[29−31] The corresponding
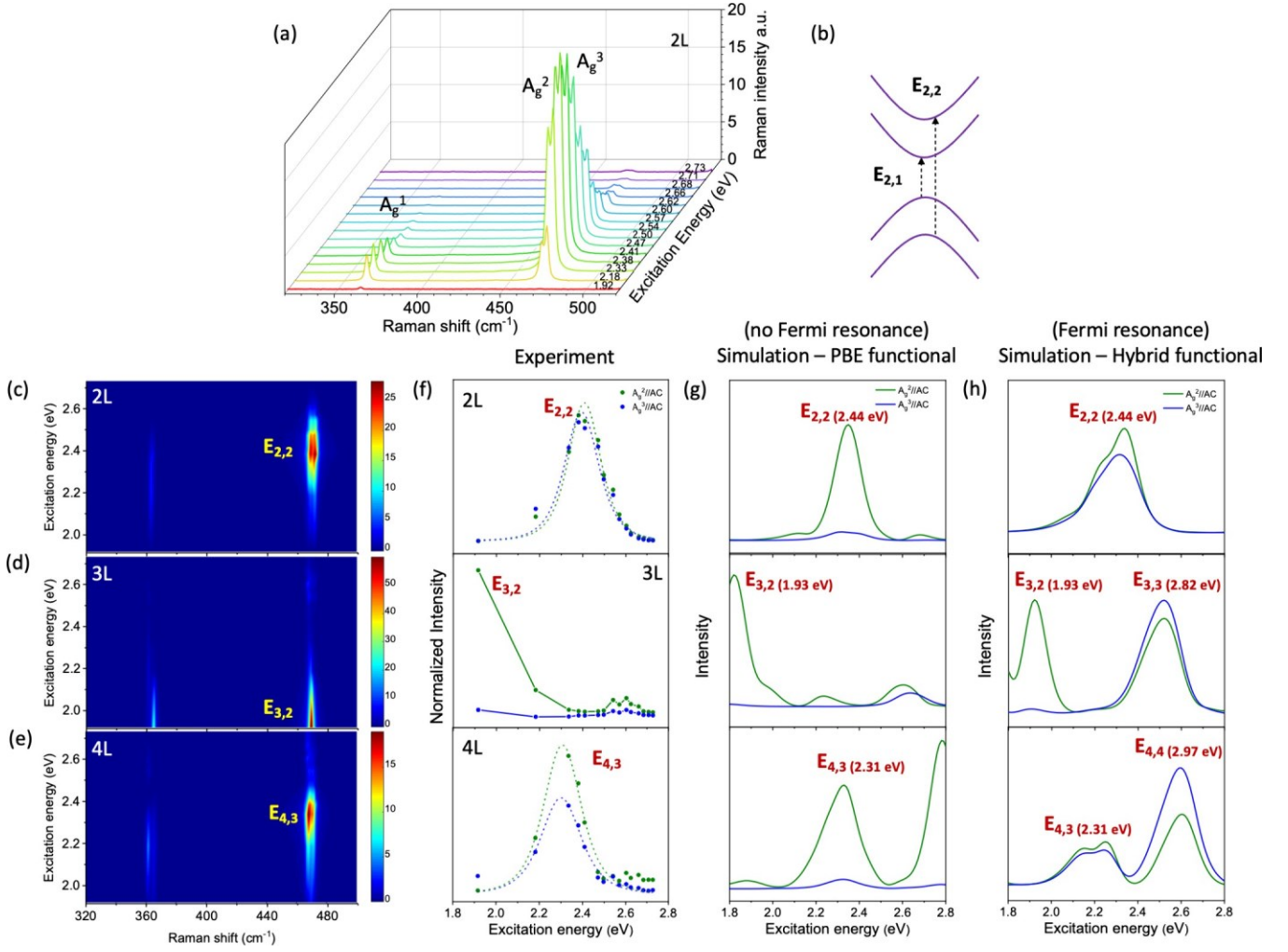
Figure 3. Electronic resonance enhancement of Fermi doublets, A_g^2 and A_g^3 modes. (a) Excitation-energy-dependent Raman spectra of 2L BP with e_i //e_s //AC configuration. (b) Schematic illustrations of optical transitions between quantized subbands of 2L BP, where $E_{2,1}$ is the band gap energy and $E_{2,2}$ represents the second electronic transition. (c–e) Measured excitation energy dependent Raman spectra of 2L–4L BP. (f) Experimental Raman excitation profiles of A_g^2 (green) and A_g^3 (blue) modes. Each green or blue dot represents one excitation laser line, and the dashed lines are the fitting results by the Fermi golden rule for a third-order time dependent perturbation theory (see Table S2). The solid line is a guide for the eye. (g,h) Simulated Raman excitation profiles of A_g^2 and A_g^3 modes by the (g) PBE method and (h) hybrid functional (PBE0) method, representing the results without and with considering Fermi coupling between these two modes. Please note that the Raman intensities and excitation energies for the PBE method (g) were computed at the *GW+BSE* level. In contrast, the simulated resonance energies using the hybrid functional (h) are slightly underestimated, compared to the electronic transitions in a previous experimental report[29] (marked by red in (g,h)).

Raman spectra for 2L BP are displayed in Figure 3a. Notably, regardless of the excitation wavelength, the A_g^3 mode consistently shows Raman intensity comparable to that of the A_g^2 mode. This consistency implies the presence of Fermi-coupling-induced wave function mixing, ultimately leading to redistribution of oscillator strength and vibration similarity between these two modes. Both modes exhibit the highest Raman intensity at an excitation energy of 2.38 eV, which aligns well with the second electronic transition ($E_{2,2}$, 2.4 eV) in 2L BP (Figure 3b).

Thickness-Dependent Fermi Resonance. Figure 3c–e displays 2D maps of the excitation-energy-dependent Raman spectra in 2L–4L BP. The corresponding resonance Raman excitation profiles (REPs) of A_g^2 and A_g^3 modes are shown in Figure 3f. For the 2L BP, the 2D map directly visualizes the excitonic resonance enhancement at $E_{2,2}$ for both A_g^2 and A_g^3 modes. Their resonance Raman exciton profiles (REPs)

overlap with each other in the investigated energy window (Figure 3f), indicating a high vibrational similarity between them (Figure 1e). However, DFT simulations using the Perdew–Burke–Ernzerhof (PBE) functional only reproduce the resonance peak on the REPs of the A_g^2 mode but not for the A_g^3 mode (Figure 3g). Without considering Fermi resonance, A_g^3 is expected to appear with weak intensity since it corresponds to a Davydov component of a Raman-inactive mode B_{2u}, as demonstrated by our PBE calculations and prior theoretical works.[35] This suggests that the PBE method fails to capture the Fermi resonance coupling between A_g^2 and A_g^3 modes, as further demonstrated by the fact that these two modes are energetically nondegenerate by this method (with ~14 cm^{-1} frequency difference) and also show different vibration patterns in PBE calculations (Figures 1e and S3).[33,35] To capture the effects of Fermi resonance in BP, it was necessary to adopt a more accurate hybrid functional
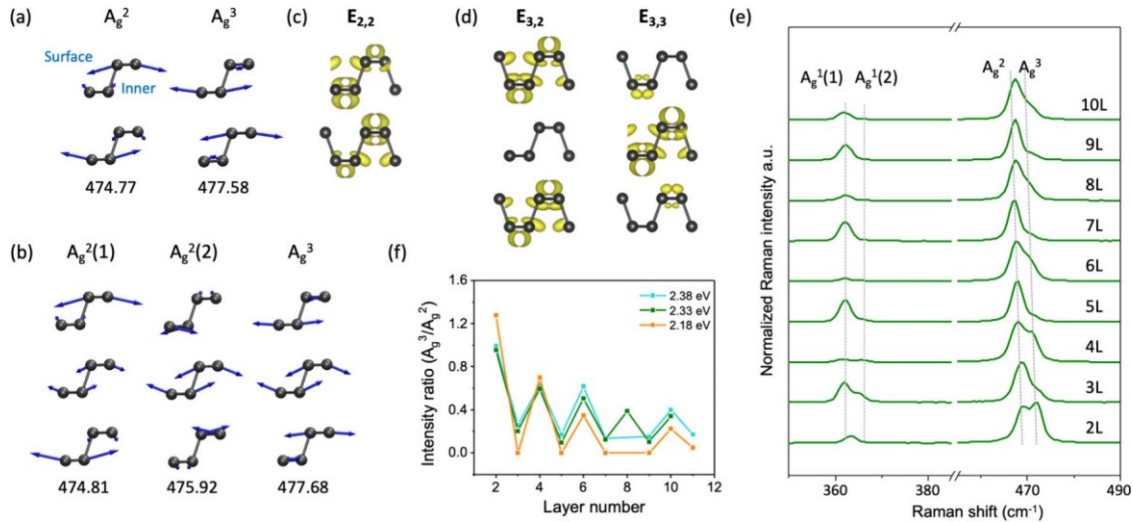
Figure 4. Thickness dependence of electronic resonance effects. (a) Calculated atomic eigen displacements and Raman frequencies of A_g^2 and A_g^3 modes in 2L BP using the hybrid functional. (b) Calculated atomic eigen displacements and Raman frequencies of A_g^2 (1), A_g^2 (2), and A_g^3 modes in 3L BP using the hybrid functional. (c) Spatial charge distribution of the excited electronic state in 2L BP. (d) Electron wave function distribution at $E_{3,2}$ and $E_{3,3}$ in 3L BP. (e) Thickness-dependent Raman spectra of few-layer BP (2L-10L) at 2.33 eV excitation energy. These Raman spectra were normalized by the intensity of the A_g^2 mode. The two Raman peaks (A_g^1(1) and A_g^1(2)) appearing around 365 cm^{-1} are the Davydov components of the A_g^1 mode. (f) Thickness-dependent intensity ratio between Fermi doublets A_g^2 and A_g^3.

method, i.e., PBE0, which not only reproduces the more accurate frequencies of A_g^2 and A_g^3 modes but also captures the strong Fermi resonance coupling between them. The hybrid functional simulated REPs of the A_g^2 and A_g^3 modes are displayed in Figure 3h. They look similar in 2L BP with a strong resonance peak around $E_{2,2}$ (2.4 eV).

For 3L BP, only the A_g^2 mode shows strong resonance effect around the second subband transition ($E_{3,2}$), while the A_g^3 mode does not (Figure 3f). The simulated REPs using the hybrid functional match well with the experimental observations. We note that a strong resonance effect of A_g^3 is predicted at the third subband transition ($E_{3,3}$) instead of $E_{3,2}$ (Figure 3h), but this is out of our experimental laser excitation range. The calculated resonance energies by the hybrid functional method are also slightly lower than the experimental energies (marked by red in Figure 3h). Such underestimation is more notable for the higher subband transitions $E_{3,3}$, whose calculated value is 2.52 eV and measured at 2.82 eV by absorption measurement.[29]

Dramatically, both modes show a strong resonance effect around the third subband transition ($E_{4,3}$) in 4L BP (Figure 3f). However, the resonance enhancement of A_g^3 is slightly weaker than that of the A_g^2 mode at $E_{4,3}$, suggesting different vibrational behaviors and electronic resonance effects for both modes. Similarly, the hybrid functional simulation reproduces the strong resonance enhancement of the A_g^3 mode (Figure 3h), while the PBE calculation does not (Figure 3g), further demonstrating that the PBE functional calculation does not capture the Fermi coupling between A_g^2 and A_g^3 modes.

To understand the electronic resonance behavior of the Fermi doublets A_g^2 and A_g^3, we compared their vibration patterns and polarizability change to the associated electron wave function distribution. The vibration patterns of A_g^2 and A_g^3 modes of 2L and 3L BP with and without considering Fermi coupling are calculated by hybrid functional (Figure 4a and b) and PBE methods (Figures 1e and S3), respectively. We can see that without considering Fermi coupling (PBE method) these two modes in 2L BP have different vibrational

patterns. The effective polarizability change of the A_g^3 mode largely gets canceled and remains almost zero, whereas there is a significant net polarizability change for the case with considering Fermi resonance (Supporting Information Note 3, Figure S4, Table S3). After Fermi resonance coupling, their vibration patterns become similar, but the displacement of P atoms is primarily localized at the surface layer for the A_g^2 mode and the inner layer for the A_g^3 mode (Figure 4a). Notably, the calculated exciton wave function at $E_{2,2}$ is distributed across the surface and inner layers (Figure 4c). The exciton probability density distribution respective to the similar atomic displacement leads to robust exciton–phonon coupling, which is revealed by the equally strong electronic resonance enhancement for the A_g^2 and A_g^3 modes in the Raman spectrum.

For 3L BP, there are two Raman-active Davydov components of A_g^2 modes (A_g^2 (1) and A_g^2 (2), Figure 4b), and both modes will interact with the A_g^3 mode. Consequently, three Raman modes are involved in the Fermi coupling (Figure 4b). However, the vibration pattern of the A_g^3 mode in the top and bottom layers largely retains the pattern after Fermi coupling, so the Fermi resonance effect is mostly reflected in the middle layer for the A_g^3 mode. According to simulation, the effective polarizability change of A_g^3 gets largely canceled for the top and bottom layer but is dominant in the middle layer (see details in Supporting Information Note 3, Figure S5, Table S4). Notably, the simulated exciton wave function density is primarily localized on the top and bottom layer for $E_{3,2}$ and on the middle layer for $E_{3,3}$ (Figure 4d) in 3L BP. Therefore, the A_g^3 mode shows weaker (stronger) electron–phonon coupling, which consequently translates into weak (strong) electronic enhancement at $E_{3,2}$ ($E_{3,3}$). In contrast, for A_g^2(1) and A_g^2(2), the atomic displacements from both the surface and the middle BP layers contribute to the Raman polarizability. Therefore, both show a strong resonance enhancement at $E_{3,2}$ and $E_{3,3}$ (Figure 3h). Discussion of 4L BP (Figure S6) can be found in the Supporting Information Note 3.

Electronic resonance effects combined with Fermi coupling lead to interesting thickness-dependent trends in the few-layer BP Raman spectrum (Figure 4e and f). For instance, the intensity ratio of A_g^3 and A_g^2 (that is, A_g^3/A_g^2) measured at the excitation energies of 2.18, 2.33, and 2.38 eV shows periodic odd−even variation with sample thickness. The ratio of A_g^3/A_g^2 is the largest for 2L BP and decreases monotonically for larger even-layer thicknesses, while the ratio is nearly zero for all odd-layer thicknesses (Figure 4f).

Finally, it is important to note that our electronic resonance data show that the Fermi resonance does not automatically guarantee comparable Raman intensities between the Fermi doublets for semiconducting systems such as BP. For 3L and other odd-layer BP, both our experimental and calculated results demonstrate that although the Fermi resonance coupling leads to similar vibrational patterns and phonon frequencies between A_g^2 and A_g^3 modes the A_g^3 mode can be still significantly weaker than the A_g^2 mode at some laser excitation energies due to the specific exciton charge distribution at these excitation energies. This means that identification of Fermi resonances in materials exhibiting sharp electronic resonances (such as atomically thin semiconductors) requires careful consideration of the electronic resonance effect.

The present work reports a Fermi resonance effect between two fundamental Raman modes in 2D few-layer black phosphorus, which gives rise to the strong Raman intensity for a Davydov component of an infrared mode. This Fermi coupling was directly demonstrated by biaxial strain-dependent Raman spectra. Moreover, the dispersive semiconducting nature and unique thickness-tunable electronic transitions of BP make it possible to investigate the excitonic effect on Fermi doublets. The thickness-dependent electronic enhancement of both Fermi doublets indicates strong wave function mixing of both unperturbed modes, which is further explained by hybrid function simulation with considering the exciton distribution with respect to the phonon vibration pattern. Our work demonstrates that Fermi resonance can provide valuable insights into the electron−phonon coupling in 2D semi-conductors.

◼ EXPERIMENTAL SECTION

Sample Preparation and Thickness Determination. Few-layer black phosphorus (BP) was exfoliated in an argon glovebox (O_2 < 0.1 ppm, H_2O < 0.1 ppm) from bulk BP crystal (HQ graphene) onto a 285 nm SiO_2/Si silicon substrate or polydimethylsiloxane (PDMS) substrate.[43] They were transferred from a PDMS substrate to a polypropylene (PP) substrate[43] for strain-dependent Raman measurement. Sample thickness was determined by optical contrast and photoluminescence spectra, as demonstrated in a previous report.[28]

Raman Measurements. Polarized Raman spectra were measured on a triple-grating Raman system (Horiba JY T64000) with 15 different excitation lines (454−648 nm, Coherent Innova 70C, Kr+−Ar+ laser). Few-layer BP was sealed in a container filled with argon gas during the Raman measurement. Raman signals were collected by a 60X objective lens (Olympus, NA = 0.7, with correction ring), dispersed by 1800 g/mm grating, and further detected by a liquid nitrogen-cooled charge couple detector (CCD). The laser power was kept below 0.54 mW for the 648 nm excitation and 0.32 mW for the high-energy excitations (454−568 nm). All spectra except strain-related experiments were collected under a parallel polarization where the incident and collection polarizations are parallel to armchair crystalline orientation of the few-layer BP. The Raman peak of single crystal quartz at 465 cm^{-1} was used to calibrate the instrument efficiency and incident power at different wavelengths.

Details on strain-dependent Raman measurements and DFT simulations can be found in the Supporting Information.

◼

■ REFERENCES

(1) Asundi, R. K.; Padhye, M. E. Fermi Resonance in Benzene. *Nature* 1949, *163* (4147), 638−638.

(2) Yagi, K.; Hirata, S.; Hirao, K. Vibrational quasi-degenerate perturbation theory: applications to fermi resonance in CO2, H2CO, and C6H6. *Phys. Chem. Chem. Phys.* 2008, *10* (13), 1781−1788.

(3) Lipp, M. J.; Yoo, C. H.; Strachan, D.; Daniels, W. B. Band-structure parameters and Fermi resonances of exciton-polaritons in CsI and CsBr under hydrostatic pressure. *Phys. Rev. B* 2006, *73* (8), 085121.

(4) Mashkovich, E. A.; Grishunin, K. A.; Dubrovin, R. M.; Zvezdin, A. K.; Pisarev, R. V.; Kimel, A. V. Terahertz light−driven coupling of antiferromagnetic spins to lattice. *Science* 2021, *374* (6575), 1608−1611.

(5) Hioki, T.; Hashimoto, Y.; Saitoh, E. Coherent oscillation between phonons and magnons. *Communications Physics* 2022, *5* (1), 115.

(6) Arranz, F. J.; Seidel, L.; Giralda, C. G.; Benito, R. M.; Borondo, F. Scars at the edge of the transition from order to chaos in the isomerizing molecular systems LiNC-LiCN and HCN-HNC, and ${\text{HO}}_{2}. *Phys. Rev. E* 2010, *82* (2), 026201.

(7) Yi, C.-H.; Yu, H.-H.; Lee, J.-W.; Kim, C.-M. Fermi resonance in optical microcavities. *Phys. Rev. E* 2015, *91* (4), 042903.

(8) Fermi, E. Über den Ramaneffekt des Kohlendioxyds. *Zeitschrift für Physik* 1931, *71* (3), 250−259.

(9) Adel, A.; Dennison, D. M. The Infrared Spectrum of Carbon Dioxide. Part I. *Phys. Rev.* 1933, *43* (9), 716−723.

(10) Scott, J. F. Evidence of Coupling Between One- and Two-Phonon Excitations in Quartz. *Phys. Rev. Lett.* 1968, *21* (13), 907−910.

(11) Bertran, J. F.; Ballester, L.; Dobrihalova, L.; Sánchez, N.; Arrieta, R. Study of Fermi resonance by the method of solvent variation. *Spectrochimica Acta Part A: Molecular Spectroscopy* 1968, *24* (11), 1765−1776.

(12) Monecke, J. Theory of Fermi resonances in Raman and infrared spectra. *J. Raman Spectrosc.* 1987, *18* (7), 477−479.

(13) Dixon, R. N. Anomalous Band Intensity in Fermi Resonance. *J. Chem. Phys.* 1959, *31* (1), 258−260.

(14) Stride, J. A.; Dallin, P. H.; Jayasooriya, U. A. Intermolecular Fermi resonance. *J. Chem. Phys.* 2003, *119* (5), 2747−2752.

(15) Schwartz, M.; Wang, C. H. Raman study of Fermi resonance, hydrogen bonding, and molecular reorientation in liquid ammonia. *J. Chem. Phys.* 1973, *59* (10), 5258−5267.

(16) Sokołowska, A.; Kęcki, Z. Inter- and intra-molecular coupling and Fermi resonance in the Raman spectra of liquid water. *J. Raman Spectrosc.* 1986, *17* (1), 29−33.

(17) Lipkin, J. S.; Song, R.; Fenlon, E. E.; Brewer, S. H. Modulating Accidental Fermi Resonance: What a Difference a Neutron Makes. *J. Phys. Chem. Lett.* 2011, *2* (14), 1672−1676.

(18) Zhelyaskov, V.; Georgiev, G.; Nickolov, Z. Temperature study of intra- and inter-molecular coupling and Fermi resonance constants in the Raman spectra of liquid water using Fourier deconvolution. *J. Raman Spectrosc.* 1988, *19* (6), 405−412.

(19) Lalov, I. J. Temperature Fermi Resonance in Crystals. *Spectrosc. Lett.* 1985, *18* (7), 555−572.

(20) Vennari, C. E.; Williams, Q. A high-pressure Raman study of FeTiO3 ilmenite: Fermi resonance as a manifestation of Fe-Ti charge transfer. *Phys. Chem. Miner.* 2021, *48* (9), 34.

(21) Sherman, W. F.; Smulovitch, P. P. Pressure-Scanned Fermi Resonance in the Spectrum of NH4+ Isolated in CsBr. *J. Chem. Phys.* 1970, *52* (10), 5187−5193.

(22) Kwon, Y.; Lee, C.; Park, S. Effect of ion−molecule interaction on fermi-resonance in acetonitrile studied by ultrafast vibrational spectroscopy. *Chem. Phys.* 2014, *445*, 38−45.

(23) Rather, S. R.; Bezdek, M. J.; Chirik, P. J.; Scholes, G. D. Dinitrogen Coupling to a Terpyridine-Molybdenum Chromophore Is Switched on by Fermi Resonance. *Chem.* 2019, *5* (2), 402−416.

(24) del Corro, E.; Terrones, H.; Elias, A.; Fantini, C.; Feng, S.; Nguyen, M. A.; Mallouk, T. E.; Terrones, M.; Pimenta, M. A. Excited excitonic states in 1L, 2L, 3L, and bulk WSe2 observed by resonant Raman spectroscopy. *ACS Nano* 2014, *8* (9), 9629−9635.

(25) Saito, R.; Fantini, C.; Jiang, J. Excitonic States and Resonance Raman Spectroscopy of Single-Wall Carbon Nanotubes. In *Carbon Nanotubes: Advanced Topics in the Synthesis, Structure, Properties and Applications*; Jorio, A., Dresselhaus, G., Dresselhaus, M. S., Eds.; Springer Berlin Heidelberg: Berlin, Heidelberg, 2008; pp 251−286.

(26) Carvalho, B. R.; Malard, L. M.; Alves, J. M.; Fantini, C.; Pimenta, M. A. Symmetry-Dependent Exciton-Phonon Coupling in 2D and Bulk MoS2 Observed by Resonance Raman Scattering. *Phys. Rev. Lett.* 2015, *114* (13), 136403.

(27) Mao, N.; Wang, X.; Lin, Y.; Sumpter, B. G.; Ji, Q.; Palacios, T.; Huang, S.; Meunier, V.; Dresselhaus, M. S.; Tisdale, W. A.; Liang, L.; Ling, X.; Kong, J. Direct Observation of Symmetry-Dependent

Electron−Phonon Coupling in Black Phosphorus. *J. Am. Chem. Soc.* 2019, *141* (48), 18994−19001.

(28) Mao, N.; Lin, Y.; Bie, Y. Q.; Palacios, T.; Liang, L.; Saito, R.; Ling, X.; Kong, J.; Tisdale, W. A. Resonance-Enhanced Excitation of Interlayer Vibrations in Atomically Thin Black Phosphorus. *Nano Lett.* 2021, *21* (11), 4809−4815.

(29) Li, L.; Kim, J.; Jin, C.; Ye, G. J.; Qiu, D. Y.; da Jornada, F. H.; Shi, Z.; Chen, L.; Zhang, Z.; Yang, F.; Watanabe, K.; Taniguchi, T.; Ren, W.; Louie, S. G.; Chen, X. H.; Zhang, Y.; Wang, F. Direct observation of the layer-dependent electronic structure in phosphorene. *Nat. Nanotechnol.* 2017, *12* (1), 21−25.

(30) Zhang, G.; Chaves, A.; Huang, S.; Wang, F.; Xing, Q.; Low, T.; Yan, H. Determination of layer-dependent exciton binding energies in few-layer black phosphorus. *Sci. Adv.* 2018, *4* (3), No. eaap9977.

(31) Zhang, G.; Huang, S.; Chaves, A.; Song, C.; Özçelik, V. O.; Low, T.; Yan, H. Infrared fingerprints of few-layer black phosphorus. *Nat. Commun.* 2017, *8*, 14071.

(32) Xia, F.; Wang, H.; Jia, Y. Rediscovering black phosphorus as an anisotropic layered material for optoelectronics and electronics. *Nat. Commun.* 2014, *5*, 4458.

(33) Cai, Y.; Ke, Q.; Zhang, G.; Feng, Y. P.; Shenoy, V. B.; Zhang, Y.-W. Phosphorene: Giant Phononic Anisotropy and Unusual Anharmonicity of Phosphorene: Interlayer Coupling and Strain Engineering (Adv. Funct. Mater. 15/2015). *Adv. Funct. Mater.* 2015, *25* (15), 2343−2343.

(34) Hu, Z.-X.; Kong, X.; Qiao, J.; Normand, B.; Ji, W. Interlayer electronic hybridization leads to exceptional thickness-dependent vibrational properties in few-layer black phosphorus. *Nanoscale* 2016, *8* (5), 2740−2750.

(35) Sun, Y.-Y.; Zhang, S. Communication: Effect of accidental mode degeneracy on Raman intensity in 2D materials: Hybrid functional study of bilayer phosphorene. *J. Chem. Phys.* 2016, *145* (2), 021102.

(36) Ikezawa, M.; Kondo, Y.; Shirotani, I. Infrared Optical-Absorption Due to One and 2 Phonon Processes in Black PhosphoruS. *J. Phys. Soc. Jpn.* 1983, *52* (5), 1518−1520.

(37) Sugai, S.; Ueda, T.; Murase, K. Pressure Dependence of the Lattice Vibration in the Orthorhombic and Rhombohedral Structures of Black Phosphorus. *J. Phys. Soc. Jpn.* 1981, *50* (10), 3356−3361.

(38) Sugai, S.; Shirotani, I. Raman and infrared reflection spectroscopy in black phosphorus. *Solid State Commun.* 1985, *53* (9), 753−755.

(39) Phaneuf-L'Heureux, A. L.; Favron, A.; Germain, J. F.; Lavoie, P.; Desjardins, P.; Leonelli, R.; Martel, R.; Francoeur, S. Polarization-Resolved Raman Study of Bulk-like and Davydov-Induced Vibrational Modes of Exfoliated Black Phosphorus. *Nano Lett.* 2016, *16* (12), 7761−7767.

(40) Kim, K.; Lee, J. U.; Nam, D.; Cheong, H. Davydov Splitting and Excitonic Resonance Effects in Raman Spectra of Few-Layer MoSe2. *ACS Nano* 2016, *10* (8), 8113−8120.

(41) Yamamoto, M.; Wang, S. T.; Ni, M.; Lin, Y.-F.; Li, S.-L.; Aikawa, S.; Jian, W.-B.; Ueno, K.; Wakabayashi, K.; Tsukagoshi, K. Strong Enhancement of Raman Scattering from a Bulk-Inactive Vibrational Mode in Few-Layer MoTe2. *ACS Nano* 2014, *8* (4), 3895−3903.

(42) Tonndorf, P.; Schmidt, R.; Böttger, P.; Zhang, X.; Börner, J.; Liebig, A.; Albrecht, M.; Kloc, C.; Gordan, O.; Zahn, D. R. T.; Michaelis de Vasconcellos, S.; Bratschitsch, R. Photoluminescence emission and Raman response of monolayer MoS2, MoSe2, and WSe2. *Opt. Express* 2013, *21* (4), 4908−4916.

(43) Huang, S.; Zhang, G.; Fan, F.; Song, C.; Wang, F.; Xing, Q.; Wang, C.; Wu, H.; Yan, H. Strain-tunable van der Waals interactions in few-layer black phosphorus. *Nat. Commun.* 2019, *10* (1), 2447.